Direct observation of reversible liquid–liquid transition in a trehalose aqueous solution

Yoshiharu Suzuki[a,1]

[a]Research Center for Advanced Measurement and Characterization, National Institute for Materials Science, Tsukuba, Ibaraki 305-0044, Japan

Edited by Pablo Debenedetti, Dean for Research, Princeton University, Princeton, NJ; received July 21, 2021; accepted December 15, 2021

Water forms two glassy waters, low-density and high-density amorphs, which undergo a reversible polyamorphic transition with the change in pressure. The two glassy waters transform into the different liquids, low-density liquid (LDL) and high-density liquid (HDL), at high temperatures. It is predicted that the two liquid waters also undergo a liquid–liquid transition (LLT). However, the reversible LLT, particularly the LDL-to-HDL transition, has not been observed directly due to rapid crystallization. Here, I prepared a glassy dilute trehalose aqueous solution (0.020 molar fraction) without segregation and measured the isothermal volume change at 0.01 to 1.00 GPa below 160 K. The polyamorphic transition and the glass-to-liquid transition for the high-density and low-density solutions were examined, and the liquid region where both LDL and HDL existed was determined. The results show that the reversible polyamorphic transition induced by the pressure change above 140 K is the LLT. That is, the transition from LDL to HDL is observed. Moreover, the pressure hysteresis of LLT suggests strongly that the LLT has a first-order nature. The direct observation of the reversible LLT in the trehalose aqueous solution has implications for understanding not only the liquid–liquid critical point hypothesis of pure water but also the relation between aqueous solution and water polyamorphism.

liquid–liquid transition | trehalose aqueous solution | polyamorphic transition | glass-to-liquid transition | water

There are at least two glassy forms of water, low-density amorph (LDA) and high-density amorph (HDA), at low temperatures (1, 2). Amman-Winkel et al. (3) have experimentally shown that the glass transition temperatures (T_g) of LDA and HDA at 1 atm are different, suggesting that low-density liquid (LDL) and high-density liquid (HDL) exist independently. In addition, the existence of metastable HDL under high pressure has been shown experimentally (4). On the other hand, computer simulation studies using several water potential models have suggested that there are two different liquid waters and that they undergo the first-order liquid–liquid transition (LLT) (5–11). Several experimental results for two glassy waters and supercooled liquid water reported so far have strongly suggested the validity of the LLT in water, although the direct observation of LLT is difficult due to the rapid crystallization. There are some reports of the transition from HDL to LDL (3, 12–16). However, the transition from LDL to HDL has not been observed directly, and the reversible LLT not only in pure water but also, in aqueous solutions, except for confined water (16), has not been observed. Therefore, direct experimental verification of reversible LLT is important for understanding the general properties of water itself, such as the anomalous behaviors of supercooled liquid water and the polyamorphic behavior of two glassy waters.

Rapid crystallization of water is a cause of difficulty in the direct observation of liquid state below the homogeneous nucleation temperature. To avoid crystallization, experimental studies on water polyamorphism using the aqueous solution system have been carried out (14, 17–33). However, the experimental reports are few because of two main reasons as follows. One is that it is difficult to vitrify dilute aqueous solutions without segregation. Since the polyamorphic behavior of aqueous solution appears only in the low-concentration region (14, 34), it is necessary to prepare the nonsegregated glass in which the solutes disperse homogeneously. Generally, when the dilute aqueous solution is cooled under ambient pressure, it segregates easily into water-rich crystalline hexagonal ice (ice Ih) and a solute-rich glassy aqueous solution called the freeze concentrated solution. Therefore, it is difficult to examine the concentration dependence of polyamorphic behaviors for the dilute aqueous solution system because of the concentration inhomogeneity induced by segregation. Another reason is that the high-pressure experiment, which is an indispensable method for the study of water polyamorphism, requires highly specialized skills and rich experiences. For a reliable evaluation of polyamorphic behaviors and a correct distinction of polyamorphic phenomena from crystallization and phase separation, it is not enough to observe the state change with the temperature change at ambient pressure, but it is necessary to verify it by measuring the state change under high pressure. However, there are few high-pressure experiments relating to the polyamorphism study of pure water and aqueous solutions (4, 12–16, 28–31, 33). For these reasons, experimental studies on the LLT in aqueous solution have been rarely performed, although the aqueous solution has the advantage of being hard to crystallize.

Several high-pressure experimental studies on the polyamorphic transition in dilute aqueous solutions have been reported (14, 27–30). We have prepared the nonsegregated glass of polyol aqueous solutions below the eutectic concentration (x_e) using a pressure liquid cooling vitrification (PLCV) method (35, 36) and examined the polyamorphic transitions with the change in pressure (14, 28–30). From the temperature, concentration, and

Significance

Recent studies on liquid water suggest that the two liquid waters exist in the supercooled temperature region and that their existence relates to the anomalous behavior of low-temperature liquid water such as the maximum density at 4 °C. However, the experimental investigation of two liquid waters is difficult because of the rapid crystallization. In this study, a reversible liquid–liquid transition in a trehalose aqueous solution by the change in pressure was observed directly. This result suggests strongly that two liquid waters exist in the aqueous solution. This study has implications for wide fields related to liquid water, such as solution chemistry, cryobiology, meteorology, and food engineering.

Author contributions: Y.S. designed research, performed research, analyzed data, and wrote the paper.

The author declares no competing interest.

This article is a PNAS Direct Submission.

[1]Email: suzuki.yoshiharu@nims.go.jp.

This article contains supporting information online at http://www.pnas.org/lookup/suppl/doi:10.1073/pnas.2113411119/-/DCSupplemental.

Published January 24, 2022.

solute nature dependences of the polyamorphic transition, we have estimated the position of the equilibrium LLT line for polyol aqueous solutions. As the solute concentration approaches zero, the position of LLT line seems to be extrapolated continuously to that of bulk pure water. This suggests that the polyamorphic transition of polyol aqueous solutions below x_e is consistently relating to that of bulk pure water.

Moreover, we have proposed a possibility that the polyamorphic transition of glycerol aqueous solution of 0.02 molar fraction is a reversible LLT (14). When the high-density glass of thew glycerol aqueous solution is decompressed from 0.6 GPa at 150 K, it changes from glass to liquid at ∼0.23 GPa, and then, it transforms to the low-density solution (LDS) at 0.16 to 0.17 GPa. When the low-density sample is compressed at the same temperature, it transforms to the original high-density solution (HDS) around 0.26 GPa. The reversible polyamorphic transition at 150 K induced by the pressure change suggests a possibility of LLT. However, the experimental evidence that both the low-density and high-density states before and after the polyamorphic transition are real liquid states has not been sufficiently ascertained. In particular, there is no experimental evidence that the low-density state at 150 K is fluid liquid.

In this study, I vitrified the emulsified trehalose aqueous solutions (TRaq solutions) of 0.015, 0.020, and 0.025 molar fractions using PLCV and examined the polyamorphic transition between the HDS and the LDS in the pressure region between 0.01 and 1.00 GPa below 160 K. Additionally, I investigated the glass-to-liquid transitions of LDS and HDS. It was found that the LDS of TRaq solution does not crystallize until ∼160 K, which is about 10 K higher than the crystallization temperature (T_x) for glycerol aqueous solution (14) and is about 20 K higher than T_x for LDA (3). This indicates that it is able to observe the polyamorphic transition for the TRaq solution in the wider temperature–pressure region. From the relationship between the polyamorphic transition and the glass-to-liquid transition, both the liquid regions of LDS and HDS were determined, and it was shown that the polyamorphic transition occurring in both the liquid regions is the reversible LLT.

Results and Discussion

The emulsified TRaq solution (x = 0.020) was vitrified using PLCV, and then, the isothermal volume change was measured between 0.01 and 1.00 GPa below 160 K. Here, the x stands for the mole fraction of solute (*Materials and Methods*). Fig. 1 shows the compression curve (V_c) and the decompression curve (V_d) of a specific volume for the TRaq solution at 159 K. When the HDS was decompressed from 0.6 GPa, the volume started to increase rapidly at ∼0.13 GPa, and the HDS transformed to LDS. When the LDS was compressed at the same temperature, the volume started to decrease rapidly at ∼0.14 GPa, and then, the LDS transformed to the original HDS. In the case of the polyamorphic transition of the aqueous solution, it is suggested that low-density and high-density states coexist in a pressure region between the beginning and end of the polyamorphic transition (14, 37, 38). Now, the HDS-to-LDS transition pressure, P_{HtoL}, and the LDS-to-HDS transition pressure, P_{LtoH}, are defined as the middle pressure between onset and offset transition pressures for each polyamorphic transition.

The V_c and V_d measured in the temperature range between 77 and 163 K are shown in *SI Appendix*, Fig. S4. When the cycle of decompression and compression is repeated at the same temperature, the corresponding V_d or V_c curves overlap (*SI Appendix*, Fig. S5). In addition, *SI Appendix*, Fig. S5 shows that the polyamorphic transition is independent of the temperature history. This high reproducibility of the polyamorphic transition shows that the trehalose molecules are homogeneously dispersed in both HDS and LDS. If the segregation is induced by the polyamorphic transition, the polyamorphic transition will not reproduce because the polyamorphic transition depends on the concentration.

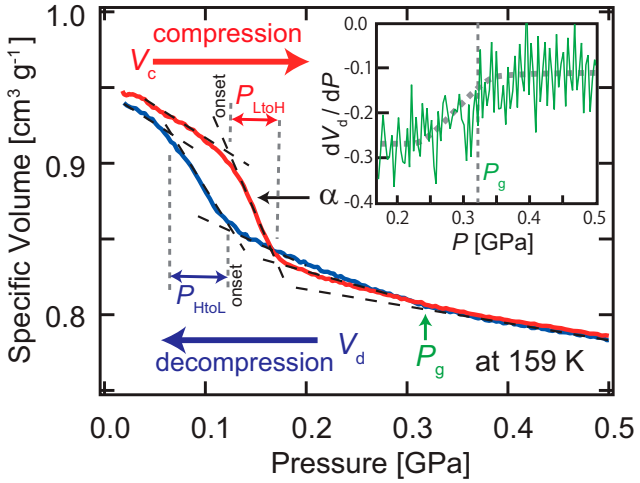

Fig. 1. The change of specific volume for the TRaq solution of x = 0.020 at 159 K with the change in pressure. The V_c and V_d are colored red and blue, respectively. P_{LtoH} and P_{HtoL} are the LDS-to-HDS transition pressure and the HDS-to-LDS transition pressure, respectively. P_g is the glass-to-liquid transition pressure of HDS; α is the absolute value of the slope of V_c during the polyamorphic transition. *Inset* represents dV_d/dP for HDS at 159 K.

The Raman spectra and powder X-ray diffraction (PXRD) patterns of HDS and LDS show that the HDS and LDS are glasses without crystalline parts and that the solvent waters of HDS and LDS relate closely to HDA and LDA of pure water, respectively (*SI Appendix*, Fig. S3). While the PXRD pattern of LDS is similar to that of pure LDA, the PXRD pattern of HDS is shifted to the lower angle side than that of pure HDA. A similar shift has been observed in other high-density aqueous solutions such as a glycerol aqueous solution (39) and a protein aqueous solution (40) as well as expanded HDA (e-HDA) (41). Kim et al. (40) have shown that the X-ray diffraction (XRD) patterns during the polyamorphic transition of the protein aqueous solution are expressed by the linear combination of LDS-XRD and HDS-XRD patterns. This suggests that the solvent water in HDS is not in an intermediate state between LDA-like water and HDA-like water, but it is close to e-HDA and is categorized as HDA.

When the HDS was decompressed at ∼162 to 165 K, a part of the LDS crystallized after or during the transformation to LDS. When the HDS was decompressed above 166K, the LDS crystallized perfectly at 0.01 GPa. The T_x of LDS for the TRaq solution is about 10 K higher than T_x of LDS for polyol aqueous solutions (14, 28, 29). When the partially crystallized low-density sample was compressed, the LDS-to-HDS polyamorphic transition of the glassy part and the pressure-induced amorphization of the crystallized part occurred at different pressures (*SI Appendix*, Fig. S10). This implies that the low-density glassy state and the crystalline state coexist independently at low pressures. A similar coexistence of the low-density glassy state and the crystalline state has been observed in the previous study for glycerol aqueous solutions (42).

Temperature dependences of P_{HtoL} and P_{LtoH} are shown in Fig. 2*A*. As the temperature increases, the P_{HtoL} shifts to the higher-pressure side, the P_{LtoH} shifts to the lower-pressure side, and the width of pressure hysteresis becomes narrower. The temperature dependence of polyamorphic behavior is consistent with that for polyol aqueous solutions (14, 28, 29).

In Fig. 1, as the pressure decreases, the slope of V_d before the polyamorphic transition becomes steeper suddenly at

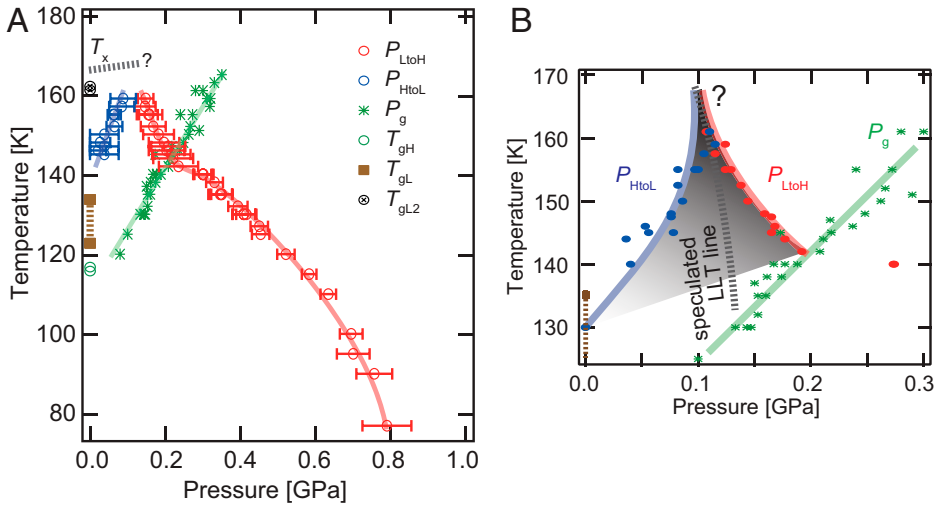

Fig. 2. Relation between the polyamorphic transition and the glass-to-liquid transition for the TRaq solution of $x = 0.020$. (*A*) The temperature dependences of P_{LtoH}, P_{HtoL}, and P_g and the T_g values of LDS and HDS at ambient pressure are shown. Red circles and blue circles are P_{LtoH} and P_{HtoL}, respectively. The edges of the error bars represent the onset and offset transition pressures. Green asterisks are P_g of HDS. T_{gH} (green circles) and T_{gL} (brown squares) are glass-to-liquid transition temperatures of HDS and LDS, respectively, which are obtained from DSC measurement at ambient pressure. T_{gL2} is the onset temperature of the endothermic event slightly before the crystallization. T_x is crystallization temperature. The red, blue, green, and brown lines are drawn to guide the eyes. (*B*) An expanded state diagram of the liquid region. The filled red circles and the filled blue circles are the onset P_{LtoH} and P_{HtoL}, respectively. Green asterisks are P_g of HDS. The red, blue, and green lines are drawn to guide the eyes. The speculated equilibrium phase boundary line of LLT is drawn as a dashed line.

P_g = ~0.32 GPa, and the dV_d/dP starts to decrease around the P_g as shown in Fig. 1, *Inset*. This means that the HDS below the P_g is softer than above the P_g, namely that the viscosity of HDS reduces suddenly at P_g in the decompression process. This suggests that HDS changes from a glassy state to a liquid state. Here, I define the P_g as the glass-to-liquid transition pressure of HDS. As shown in Fig. 2*A*, the P_g increases as the temperature increases. This suggests that the HDS existing in the lower-pressure region of the P_g curve is liquid. The change in P_g with the change in temperature for HDS is consistent with the change in T_g with the change in pressure for pure HDA (43–45).

The P_g curve intersects the P_{LtoH} curve at ~140 K as shown in Fig. 2*A*. The onset P_{LtoH} below 140 K is off to the higher-pressure side, and the LDS-to-HDS transition below 140 K appears to occur with a delay. The delay of the polyamorphic transition occurs just within the glass region of HDS. It is found that the LDS-to-HDS transition within the glass region of HDS is different from that within the liquid region of HDS. The same delayed LDS-to-HDS transitions in the glassy HDS region are also observed for TRaq solutions of different concentrations (*SI Appendix*, Fig. S6).

The difference between polyamorphic transitions within the glassy HDS region and the liquid HDS region can be seen in the difference in the slope of V_c during the LDS-to-HDS transition. For quantitative explanation, I define α as an absolute value of the slope as shown in Fig. 1, although α has no physical meaning. The temperature dependence of α is shown in Fig. 3*A* and *SI Appendix*, Fig. S8. The behavior of α changes drastically around 142 K, which agrees roughly with the temperature at which the P_g curve intersects the P_{LtoH} curve. The α for the polyamorphic transitions occurring in the liquid HDS region above 142 K increases monotonically with the increase of temperature. This suggests that the viscosity of HDS decreases with the increase of temperature, namely that the HDS changes continuously from the viscous liquid to the fluid liquid. On the other hand, the α for the polyamorphic transition occurring in the glassy HDS region below 142 K also increases with the increase of temperature, indicating that the glassy HDS becomes softer at high temperatures. However, the α slightly below 142 K is much larger than that slightly above 142 K. The remarkably large α in the glassy HDS region indicates that as soon as the polyamorphic transition starts, the volume decreases rapidly, and the polyamorphic transition completes instantly.

Now, I consider the difference between the LDS-to–liquid HDS transition and the LDS-to–glassy HDS transition. When pressure is applied to the sample in the constant compression rate, if the HDS is liquid, the change of volume can follow the change of pressure within the laboratory timescale, and the LDS-to-HDS transition will occur at the expected transition pressure (P_A in Fig. 3 *B* and *C*). On the other hand, if the HDS is glass, the change of volume cannot follow the pressure change because the HDS has high viscosity as shown by the red process of Fig. 3*B*. Therefore, the LDS-to-HDS transition cannot occur at the expected pressure (P_B in Fig. 3 *B* and *C*), will delay, and will occur at higher pressure (P_C in Fig. 3 *B* and *C*). As a result, the difference between the onset and offset transition pressures becomes smaller, and the decrease of volume looks like a collapse. In other words, the α indirectly indicates the delay of the onset transition pressure of the LDS-to-HDS transition in the glassy HDS region. The delay in polyamorphic transition below ~140 K in Fig. 2*A* and the extremely large α slightly below 142 K in Fig. 3*A* explain consistently that the LDS-to-HDS polyamorphic transition occurs in the glassy HDS region. A similar delay in the transition within the glass region has been observed in the pressure-induced melting of ice Ih by Mishima (46).

In this study, the glass-to-liquid transition of HDS was investigated by three different evaluation methods: first, the change in the slope of the decompression curve at P_g; second, the delay of the onset of the polyamorphic transition on compression; and third, the change in the slope of the compression curve during the polyamorphic transition. All the methods relate to the measurements of mechanical softening of HDS. These experimental results indicate that the HDS in the liquid region is viscous liquid with fluidity.

Next, I examined the glass-to-liquid transitions of HDS and LDS at ambient pressure using a differential scanning

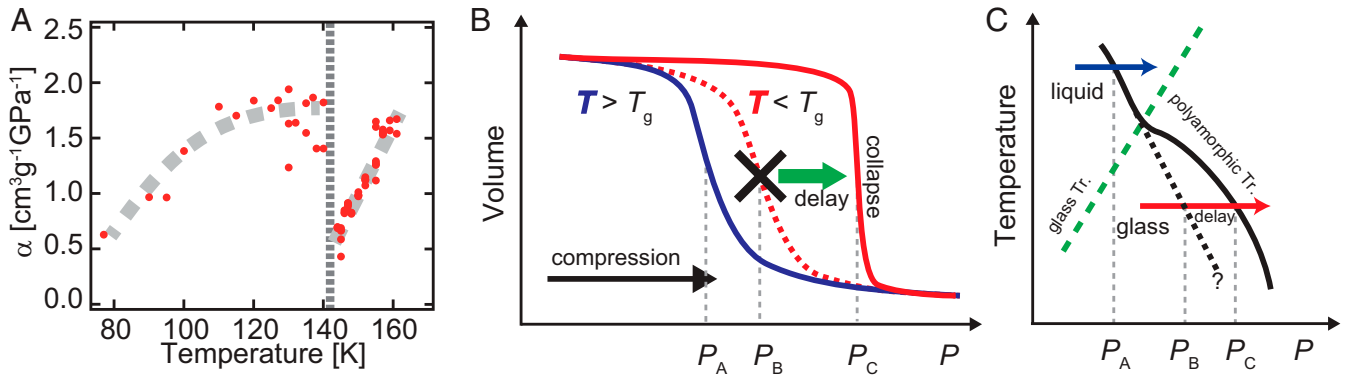

Fig. 3. Temperature dependence of α for the TRaq solution of $x = 0.020$ and the schematic explanation for the difference between polyamorphic transitions within the liquid region and within the glassy region. (*A*) Temperature dependence of α. A vertical line represents the position of 142 K. The gray curves are drawn to guide the eyes. (*B*) Schematic polyamorphic volume changes by applied pressure. The LDS-to-HDS transition within the liquid HDS region (blue) occurs at P_A. The LDS-to-HDS transition within the glassy HDS region (red) occurs at higher P_C than the expected P_B. (*C*) Relation between the P_{LtoH} and the P_g of HDS. A black dashed curve is the expected equilibrium P_{LtoH} curve. A green dashed curve is P_g of HDS.

calorimetry (DSC). Fig. 4*A* shows the DSC scans for the HDS. The HDS was repeatedly annealed three times slightly before the polyamorphic transition to LDS to avoid the effect of structural relaxation. In the first and second DSC scans, there are many small exothermic peaks due to the thermal structural relaxation of HDS. A highly reproducible endothermic event relating to glass transition occurs around 117 K in the third and fourth DSC scans. This T_g (~117 K) is in rough agreement with the temperature estimated by the extrapolation of the P_g curve to 1 atm (0.0001 GPa) (Fig. 2*A*). The T_g is higher than the T_g of HDA at ambient pressure (~110 K) reported by Amann-Winkel et al. (3). This suggests that the existence of trehalose may stabilize the HDA-like solvent water (29, 30). An exothermic event at ~142 K in the fourth DSC scan shows that the HDS transforms to LDS.

The DSC scans of LDS are shown in Fig. 4*B*. The LDS was annealed three times before the T_x. The endothermic event relating to glass transition starts around 123 K and then, finishes around 135 K. The endothermic event between 123 and 135 K is observed with good reproducibility. The temperature of the endothermic event is slightly lower than T_g (~136 K) of LDA at 1 atm (3). In addition, the T_g of LDS is lower than the T_g estimated by the extrapolation of the T_g curve for the high-concentration TRaq solutions to $x = 0.020$ (47, 48) (*SI Appendix*, Fig. S2).

The DSC intensity relating to the glass transition of pure HDA is five times greater than that of pure LDA (3), but in the case of the TRaq solution, the DSC intensities relating to the glass transition of HDS and LDS appear to be almost the same. The reason for this is not clear. I infer that perhaps this could be an effect of aqueous solution.

It is discussed whether the glass transition of LDA around 136 K determined by the calorimetry measurements is responsible for the reorientational dynamics of a water molecule or not (49–51). Direct visual observations of LDA and LDA-like aqueous solution have suggested that LDA above T_g is viscous liquid with fluidity. For example, Kim et al. (52) have observed that the crack healing in the LDA-like aqueous solution occurs above 155 K, and Mishima et al. (53) have observed that the smoothing of the phase boundary between HDA and LDA in a diamond anvil cell occurs at 145 K. These past experimental results suggest strongly that the LDS above the T_g at ambient pressure is viscous liquid with fluidity.

The behavior of the glass transition of LDS at high pressures is not clarified. Using the same estimation method of the P_g of HDS by the change in the slope of the decompression curve, I attempted to derive the P_g of LDS at high pressures in the temperature range of 112 to 144 K. Unfortunately, no significant change in the slope of the decompression curve relating to the glass transition was observed (*SI Appendix*, Fig. S9). On the other hand, the molecular dynamics simulation result reported by Giovambattista et al. (45) predicted that the T_g of LDA decreases slowly with the increase in pressure. According to their prediction, there is no doubt that the LDS at high pressures above ~135 K in Fig. 2*A* is in the viscous liquid state.

The eighth DSC scan in Fig. 4*B* shows that the LDS starts to crystallize at ~170 K. A small endothermic event was observed around 165 K, which is slightly before the crystallization. At present, the cause of the endothermic event is not clear. It may

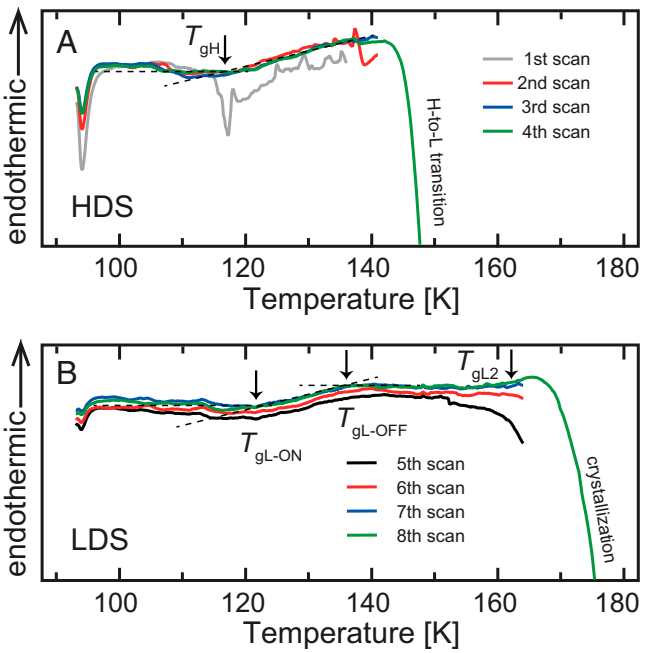

Fig. 4. DSC scans of HDS and LDS for the TRaq solution of $x = 0.020$. (*A*) DSC scans of HDS. T_{gH} is the onset glass transition temperature of HDS. (*B*) DSC scans of LDS. $T_{gL\text{-}ON}$ and $T_{gL\text{-}OFF}$ are the onset and offset glass transition temperatures of LDS. T_{gL2} is the onset temperature of the endothermic event slightly before the crystallization.

be related to the relaxation of a hydrated trehalose molecule or the nanosegregation of the aqueous solution. It is necessary to investigate this issue in the future.

Conclusions

The polyamorphic-state diagrams of the TRaq solution in Fig. 2*B* show that the viscous liquid HDS exists within the lower-pressure region of the P_g curve and that the viscous liquid LDS exists above ∼135 K at low pressures. Therefore, the polyamorphic transition occurring in both liquid regions is LLT, namely that the polyamorphic transition at 159 K shown in Fig. 1 is most likely the reversible LLT. In particular, the LLT from low-density state to high-density state was directly observed. Delay of the LDS-to-HDS transition below T_g was also observed.

The existence of pressure hysteresis for the LLT suggests that the spinodal region of LDL and the spinodal region of HDL lie in a liquid region between P_{HtoL} and P_{LtoH} (the gray region in Fig. 2*B*). It is found that the width of pressure hysteresis becomes narrow with temperature increases, which is consistent with the general phase transition phenomena. The existence of pressure hysteresis under the equilibrium condition is strong evidence that the LLT in the TRaq solution is the first-order transition. Further experiments on the dynamics related to the glass-to-liquid transition of HDS and LDS under pressure will be needed to further confirm the results in this study, such as the first-order LLT in the TRaq solution.

It is important to confirm that the LLT of TRaq solutions in the concentration range examined in this study is related to that of bulk pure water. Now, using the estimation method of the positions of LLT, which has been proposed to quantify the polyamorphic transition in polyol aqueous solutions (29), I calculated roughly the position of the LLT line for the TRaq solution at 155 K (Fig. 5 and *SI Appendix*, Fig. S7). The pressure of the LLT line increases with the decrease of x, and then, when the x approaches zero, the pressure of LLT line is extrapolated to ∼0.2 GPa. This pressure is in close agreement with the pressure of LLT predicted for pure water (∼0.2 to 0.23 GPa) (12, 29). This suggests strongly that the polyamorphic transition of TRaq solutions below the x_e consistently relates to that of bulk pure water. In short, the solvent water in the TRaq solution below the x_e inherits the nature of bulk pure water, although the solvent water is perturbated from the solute.

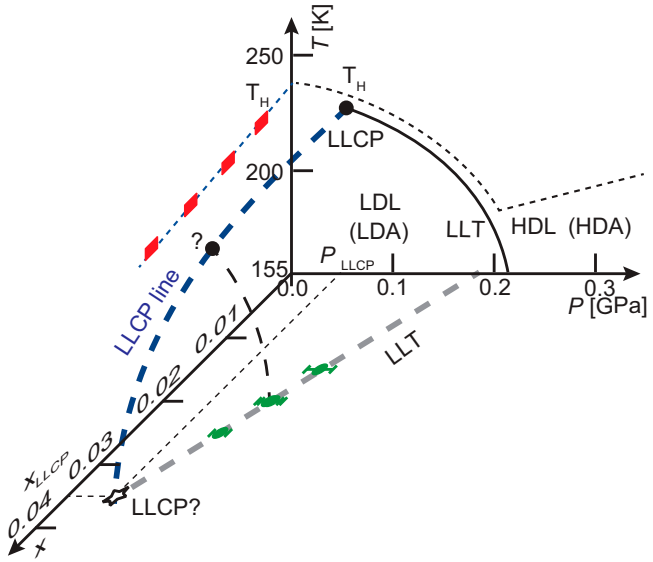

Fig. 5. *P–T–x* state diagram of solvent water in a TRaq solution from the viewpoint of water polyamorphism. The green circles represent the positions of LLT at 155 K, which are calculated from the analysis of V_c and V_d for TRaq solutions of x = 0.015, 0.020, and 0.025 (*SI Appendix*, Fig. S7). The LLCP of the TRaq solution at 155 K is speculated to locate at P_{LLCP} = ∼0.05GPa and x_{LLCP} = ∼0.035. The gray LLT curve is drawn to guide the eyes. The *P–T* state diagram of pure water is proposed by Mishima and Stanley (12). The T_H of the TRaq solution (red squares) is proposed by Miyata and Kanno (54). A blue dashed line is a speculated LLCP line of the TRaq solution.

The equilibrium phase boundary line of LDS and HDS for the TRaq solution of x = 0.020 should lie somewhere in the gray region of Fig. 2*B* and should be extended to the higher-temperature side. Although it is difficult to decide the exact position of the phase boundary line, I have attempted to estimate the positions of phase boundary and liquid-liquid critical point (LLCP) roughly from the concentration dependence of polyamorphic transition. The concentration dependence of the position of the LLT line suggests that the LLCP on the *P–x* plane at 155 K locates at x_{LLCP} = ∼0.035 and P_{LLCP} = ∼0.05 GPa (Fig. 5 and *SI Appendix*, Fig. S7). The P_{LLCP} is approximately in agreement with the P_{LLCP} of pure water (∼0.05 GPa) (12). This suggests that the P_{LLCP} for the TRaq solution changes little in response to changes in concentration. Moreover, the experimental studies of polyamorphism of water (12) and polyol aqueous solutions (29) suggest a tendency that the T_H exists near the extension of the LLT line. Assuming that the LLCP line and the T_H line have a parallel relation, the LLCP line of the TRaq solution in the *P–T–x* phase diagram may be drawn as the blue dashed line in Fig. 5 that is parallel to the T_H line of TRaq solution at 1 atm (54). As the result, the LLT line of the TRaq solution of x = 0.020 may terminate somewhere below ∼210 K at ∼0.05 GPa. However, the relation between the LLT of the TRaq solution in this study, the LLT of bulk pure water, and the estimated LLCP position of the TRaq solution requires future theoretical/computational studies.

This experimental result shows that two liquid waters exist in the aqueous solution and suggests a possibility that pure water undergoes the discontinuous LLT between LDL and HDL. In addition, this study raises the importance of considering the properties of low-temperature aqueous solutions from a viewpoint of two liquid waters and has implications for understanding the glassy water in cryobiology, frozen food engineering, meteorology, and planetology.

Materials and Methods

Preparation of the Sample. TRaq solution was prepared by mixing dihydrated trehalose ($C_{12}H_{22}O_{11}{\cdot}H_2O$; Hayashibara Co.) and water (H_2O) purified by the water purification apparatus (Merck Direct-Q UV). The solute concentrations were x = 0.015, 0.020, and 0.025, where x stands for the solute molar fraction, which is a ratio of a solute molar number to the sum of a solute molar number and a water molar number. To hinder the crystallization, 1 g of aqueous solution is emulsified by blending with a matrix (0.75 g of methylcyclohexane, 0.75 g of methylcyclopentane, 50 mg of sorbitan tristerate) for 1 min using a homogenizer (OMNI International; Omni TH) at 30,000 rpm. The emulsion size is 1 to 10 μm in diameter.

In order to vitrify the dilute TRaq solution without segregation, the PLCV method was used in this study. First, the liquid sample was sealed in an indium container at 1 atm, and the indium container was set in a piston–cylinder pressure device. The piston–cylinder device was placed in a hydraulically controlled press apparatus, and pressure of 0.3 GPa was applied to the sample at room temperature. Subsequently, the sample was cooled to 77 K with liquid nitrogen at a cooling rate of ∼40 K/min. A temperature–pressure protocol of preparation is shown in *SI Appendix*, Fig. S1.

Isothermal Volume Change Measurements under Pressure. The HDS was compressed and decompressed in the pressure range between 0.01 and 1.00 GPa in the temperature range between 77 and ∼170 K. The compression and decompression rates were fixed at 1.6 and −1.6 MPa/s, respectively. In advance, the compression and decompression curves of piston displacement, d, for only indium container of 13.000 ± 0.002 g weight were measured, and the compression and decompression curves of specific volume for only the emulsion matrix were calculated. The weight of the indium container with the emulsified solution sample was measured before the glassy sample preparation by PLCV. The

compression curve of *d* for only the indium container was subtracted from the measured compression curve of *d* for the indium container with the sample, and then, the compression curve of the specific volume of only the sample was calculated using the information of the specific volume of the emulsion matrix. Using the same method, the decompression curve of the specific volume of the sample was calculated. The specific volume is accurate to within 1.0%.

The effect of friction between piston and cylinder on the pressure value was corrected so that the compression and decompression curves of only the indium metal became the same curve. Detailed correction methods have been described in ref. 14. The absolute and relative errors of corrected pressure are $\pm\sim$0.01 and $\pm\sim$0.005 GPa, respectively.

The measurement temperature (T_{cyl}) was measured by a thermocouple in direct contact with the cylinder. The T_{cyl} was controlled by the balance between the heater attached to the cylinder and the surrounding cold nitrogen gas. Since the volume of the cylinder is much larger than the sample volume, there is little influence of the change of sample temperature due to the transformation of the sample on the stability of T_{cyl}. The stability of T_{cyl} is within $\pm\sim$0.2 K.

DSC. In order to examine the glass transitions of HDS and LDS, the low-temperature differential scanning calorimeter (Perkin-Elmer; Pyris1 with CryoFill) calibrated using both cyclopentane and *n*-heptane was used. About 25 mg of HDS was packed in a handmade aluminum pan in liquid nitrogen, and then, the pan was put in the DSC apparatus. The DSC scan was recorded upon heating from 93 K to a given temperature at 10 K/min in a flowing helium atmosphere.

In this study, I do not discuss the absolute value of heat flow in DSC measurement exactly because it is difficult to measure the accurate weight of the sample due to the packing of the sample in liquid nitrogen. Therefore, to enhance the small endothermic sign due to the glass transition, I calculated the difference between the DSC scan for the glassy sample and the DSC scan for the crystallized sample that was transformed to ice Ih at high temperature and then, discussed the glass transition from the relative changes in the slope of DSC scans. Thermodynamic discussion of the glassy states of HDS and LDS and their glass transitions by heat capacity will be a future topic.

Data Availability. All study data are included in the article and/or *SI Appendix*.

ACKNOWLEDGMENTS. I thank O. Mishima, K. Sasaki, and T. Uchida for useful comments and discussions and S. Takeya for the PXRD measurements. This work was supported by a Grant-in-Aid for Scientific Research (20K03888) from the Japan Society for the Promotion of Science.

1. O. Mishima, L. D. Calvert, E. Whalley, 'Melting ice' I at 77 K and 10 kbar: A new method of making amorphous solids. *Nature* **310**, 393–395 (1984).
2. O. Mishima, L. D. Calvert, E. Whalley, An apparently first-order transition between two amorphous phases of ice induced by pressure. *Nature* **314**, 76–78 (1985).
3. K. Amann-Winkel *et al.*, Water's second glass transition. *Proc. Natl. Acad. Sci. U.S.A.* **110**, 17720–17725 (2013).
4. J. N. Stern, M. Seidl-Nigsch, T. Loerting, Evidence for high-density liquid water between 0.1 and 0.3 GPa near 150 K. *Proc. Natl. Acad. Sci. U.S.A.* **116**, 9191–9196 (2019).
5. P. H. Poole, F. Sciortino, U. Essmann, H. E. Stanley, Phase behaviour of metastable water. *Nature* **360**, 324–328 (1992).
6. J. C. Palmer *et al.*, Metastable liquid-liquid transition in a molecular model of water. *Nature* **510**, 385–388 (2014).
7. R. S. Singh, J. W. Biddle, P. G. Debenedetti, M. A. Anisimov, Two-state thermodynamics and the possibility of a liquid-liquid phase transition in supercooled TIP4P/2005 water. *J. Chem. Phys.* **144**, 144504 (2016).
8. J. L. F. Abascal, C. Vega, Widom line and the liquid-liquid critical point for the TIP4P/2005 water model. *J. Chem. Phys.* **133**, 234502 (2010).
9. T. Yagasaki, M. Matsumoto, H. Tanaka, Spontaneous liquid-liquid phase separation of water. *Phys. Rev. E* **89**, 020301 (2014).
10. T. Sumi, H. Sekino, Effects of hydrophobic hydration on polymer chains immersed in supercooled water. *RSC Advances* **3**, 12743 (2013).
11. T. E. Gartner III *et al.*, Signatures of a liquid-liquid transition in an ab initio deep neural network model for water. *Proc. Natl. Acad. Sci. U.S.A.* **117**, 26040–26046 (2020).
12. O. Mishima, H. E. Stanley, Decompression-induced melting of ice IV and the liquid–liquid transition in water. *Nature* **392**, 164–168 (1998).
13. O. Mishima, Volume of supercooled water under pressure and the liquid-liquid critical point. *J. Chem. Phys.* **133**, 144503 (2010).
14. Y. Suzuki, O. Mishima, Experimentally proven liquid-liquid critical point of dilute glycerol-water solution at 150 K. *J. Chem. Phys.* **141**, 094505 (2014).
15. K. H. Kim *et al.*, Experimental observation of the liquid-liquid transition in bulk supercooled water under pressure. *Science* **370**, 978–982 (2020).
16. Y. Zhang *et al.*, Density hysteresis of heavy water confined in a nanoporous silica matrix. *Proc. Natl. Acad. Sci. U.S.A.* **108**, 12206–12211 (2011).
17. Y. Suzuki, O. Mishima, Two distinct raman profiles of glassy dilute LiCl solution. *Phys. Rev. Lett.* **85**, 1322–1325 (2000).
18. S.-H. Chen *et al.*, Observation of fragile-to-strong dynamic crossover in protein hydration water. *Proc. Natl. Acad. Sci. U.S.A.* **103**, 9012–9016 (2006).
19. F. Mallamace, C. Corsaro, P. Baglioni, E. Fratini, S.-H. Chen, The dynamical crossover phenomenon in bulk water, confined water and protein hydration water. *J. Phys. Condens. Matter* **24**, 064103 (2012).
20. F. Mallamace *et al.*, The influence of water on protein properties. *J. Chem. Phys.* **141**, 165104 (2014).
21. F. Mallamace *et al.*, Dynamical properties of water-methanol solutions. *J. Chem. Phys.* **144**, 064506 (2016).
22. C. U. Kim, M. W. Tate, S. M. Gruner, Protein dynamical transition at 110 K. *Proc. Natl. Acad. Sci. U.S.A.* **108**, 20897–20901 (2011).
23. Y. Yoshimura, H. Kanno, Pressure-induced amorphization of ice in aqueous LiCl solution. *J. Phys. Condens. Matter* **14**, 10671–10674 (2002).
24. I. Popov, A. Greenbaum Gutina, A. P. Sokolov, Y. Feldman, The puzzling first-order phase transition in water-glycerol mixtures. *Phys. Chem. Chem. Phys.* **17**, 18063–18071 (2015).
25. O. Andersson, A. Inaba, Glass transitions in pressure-collapsed ice clathrates and implications for cold water. *J. Phys. Chem. Lett.* **3**, 1951–1955 (2012).
26. Y. Suzuki, O. Mishima, Sudden switchover between the polyamorphic phase separation and the glass-to-liquid transition in glassy LiCl aqueous solutions. *J. Chem. Phys.* **138**, 084507 (2013).
27. Y. Suzuki, O. Mishima, Effect of water polyamorphism on the molecular vibrations of glycerol in its glassy aqueous solutions. *J. Chem. Phys.* **145**, 024501 (2016).
28. Y. Suzuki, Effect of solute nature on the polyamorphic transition in glassy polyol aqueous solutions. *J. Chem. Phys.* **147**, 064511 (2017).
29. Y. Suzuki, Experimental estimation of the location of liquid-liquid critical point for polyol aqueous solutions. *J. Chem. Phys.* **149**, 204501 (2018).
30. Y. Suzuki, Effect of OH groups on the polyamorphic transition of polyol aqueous solutions. *J. Chem. Phys.* **150**, 224508 (2019).
31. G. N. Ruiz, L. E. Bove, H. R. Corti, T. Loerting, Pressure-induced transformations in LiCl-H2O at 77 K. *Phys. Chem. Chem. Phys.* **16**, 18553–18562 (2014).
32. G. N. Ruiz, K. Amann-Winkel, L. E. Bove, H. R. Corti, T. Loerting, Calorimetric study of water's two glass transitions in the presence of LiCl. *Phys. Chem. Chem. Phys.* **20**, 6401–6408 (2018).
33. J. Bachler *et al.*, Glass polymorphism in glycerol-water mixtures. II. Experimental studies. *Phys. Chem. Chem. Phys.* **18**, 11058–11068 (2016).
34. J. Bachler, P. H. Handle, N. Giovambattista, T. Loerting, Glass polymorphism and liquid-liquid phase transition in aqueous solutions: Experiments and computer simulations. *Phys. Chem. Chem. Phys.* **21**, 23238–23268 (2019).
35. O. Mishima, Y. Suzuki, Vitrification of emulsified liquid water under pressure. *J. Chem. Phys.* **115**, 4199–4202 (2001).
36. Y. Suzuki, O. Mishima, Raman spectroscopic study of glassy water in dilute lithium chloride aqueous solution vitrified under pressure. *J. Chem. Phys.* **117**, 1673–1676 (2002).
37. J. W. Biddle, V. Holten, M. A. Anisimov, Behavior of supercooled aqueous solutions stemming from hidden liquid-liquid transition in water. *J. Chem. Phys.* **141**, 074504 (2014).
38. T. Yagasaki, M. Matsumoto, H. Tanaka, Liquid-liquid separation of aqueous solutions: A molecular dynamics study. *J. Chem. Phys.* **150**, 214506 (2019).
39. Y. Suzuki, S. Takeya, Slow crystal growth of cubic ice with stacking faults in a glassy dilute glycerol aqueous solution. *J. Phys. Chem. Lett.* **11**, 9432–9438 (2020).
40. C. U. Kim, B. Barstow, M. W. Tate, S. M. Gruner, Evidence for liquid water during the high-density to low-density amorphous ice transition. *Proc. Natl. Acad. Sci. U.S.A.* **106**, 4596–4600 (2009).
41. K. Winkel, M. S. Elsaesser, E. Mayer, T. Loerting, Water polyamorphism: Reversibility and (dis)continuity. *J. Chem. Phys.* **128**, 044510 (2008).
42. Y. Suzuki, Non-segregated crystalline state of dilute glycerol aqueous solution. *J. Chem. Phys.* **152**, 144501 (2020).
43. M. Seidl *et al.*, Volumetric study consistent with a glass-to-liquid transition in amorphous ices under pressure. *Phys. Rev. B* **83**, 100201 (2011).
44. T. Loerting *et al.*, The glass transition in high-density amorphous ice. *J. Non-Cryst. Solids* **407**, 423–430 (2015).
45. N. Giovambattista, T. Loerting, B. R. Lukanov, F. W. Starr, Interplay of the glass transition and the liquid-liquid phase transition in water. *Sci. Rep.* **2**, 390 (2012).
46. O. Mishima, Relationship between melting and amorphization of ice. *Nature* **384**, 546–549 (1996).
47. K. D. Roe, T. P. Labuza, Glass transition and crystallization of amorphous trehalose-sucrose mixtures. *Int. J. Food Prop.* **8**, 559–574 (2005).
48. T. Chen, A. Fowler, M. Toner, Literature review: Supplemented phase diagram of the trehalose-water binary mixture. *Cryobiology* **40**, 277–282 (2000).
49. C. A. Angell, Liquid fragility and the glass transition in water and aqueous solutions. *Chem. Rev.* **102**, 2627–2650 (2002).
50. M. Fisher, J. P. Devlin, Defect activity in amorphous ice from isotopic exchange data: Insight into the glass transition. *J. Phys. Chem.* **99**, 11584–11590 (1995).
51. J. J. Shephard, C. G. Salzmann, Molecular reorientation dynamics govern the glass transitions of the amorphous ices. *J. Phys. Chem. Lett.* **7**, 2281–2285 (2016).
52. C. U. Kim, M. W. Tate, S. M. Gruner, Glass-to-cryogenic-liquid transitions in aqueous solutions suggested by crack healing. *Proc. Natl. Acad. Sci. U.S.A.* **112**, 11765–11770 (2015).
53. O. Mishima, K. Takemura, K. Aoki, Visual observations of the amorphous-amorphous transition in H2O under pressure. *Science* **254**, 406–408 (1991).
54. K. Miyata, H. Kanno, Supercooling behavior of aqueous solutions of alcohols and saccharides. *J. Mol. Liq.* **119**, 189–193 (2005).